Neutrino initiated cascades at mid and high altitudes in the atmosphere

A.D. Supanitsky [a,*] and G. Medina-Tanco [a]

[a] *Instituto de Ciencias Nucleares, UNAM, Circuito Exteriror S/N, Ciudad Universitaria, México D. F. 04510, México.*

Abstract

High energy neutrinos play a very important role for the understanding of the origin and propagation of ultra high energy cosmic rays (UHECR). They can be produced as a consequence of the hadronic interactions suffered by the cosmic rays in the acceleration regions, as by products of the propagation of the UHECR in the radiation background and as a main product of the decay of super heavy relic particles. A new era of very large exposure space observatories, of which the JEM-EUSO mission is a prime example, is on the horizon which opens the possibility of neutrino detection in the highest energy region of the spectrum. In the present work we use a combination of the PYTHIA interaction code with the CONEX shower simulation package in order to produce fast one-dimensional simulations of neutrino initiated showers in air. We make a detail study of the structure of the corresponding longitudinal profiles, but focus our physical analysis mainly on the development of showers at mid and high altitudes, where they can be an interesting target for space fluorescence observatories.

Key words: Ultra High Energy Neutrinos, Space Observation
PACS:

1 Introduction

The high ($E_\nu \lesssim 10^{17}$ eV) and ultra high ($E_\nu > 10^{17}$ eV) energy neutrino fluxes carry very important astrophysical information. In particular, neutrinos arriving to the Earth can be originated in very distant sources because they travel through the universe without interacting. A high energy neutrino flux is expected as a by-product of the interactions of cosmic ray hadrons at the

* Corresponding author. E-mail: supanitsky@nucleares.unam.mx.

sources (see e.g. [1]). They can also be produced during the propagation of cosmic rays in the intergalactic medium [2,3] and as the main product of the decay of superheavy relic particles [8,9].

There are essentially two different strategies to detect neutrinos in cosmic rays detectors. The first consist in observing the development of horizontal air showers produced by the interactions of electron neutrinos with nucleons of the molecules of the Earth atmosphere [7], and the second one consist in observing the showers produced by the decay of taus generated by the interaction of tau neutrinos propagating through the interior of the Earth [4,5,6].

Space observatories play a very important role in neutrino detection, in particular, JEM-EUSO [10] with its 10^{12} tn of atmospheric target volume has the real possibility of observing ultra high energy neutrinos and make important contributions to the understanding of UHECR production and propagation [11,12]. Source distributions rapidly evolving with redshift would be particularly favorable by increasing the cosmogenic neutrino flux at highest energies [2]. A thorough understanding of neutrino deep inelastic scattering, as well as the evolution of longitudinal profiles of atmospheric neutrino showers, are extremely important in order to take advantage of the full potential of the experiment. Conversely, besides the obvious astrophysical value, the properties of just a few observed showers can also give valuable information on the physics governing high energy neutrino-nucleon interactions.

In this work we first study the neutrino-nucleon interactions at the highest energies for two different sets of parton distribution functions. We study in detail, the characteristics of horizontal air showers originated by the interactions of electron neutrinos in the Earth atmosphere. In particular, we consider horizontal showers initiated at different altitudes and very deep in the atmosphere, which, depending on the flux, will be detected by the upcoming orbital detectors like JEM-EUSO. We also study the detectability of such showers as a function of the altitude, for an ideal orbital detector similar to JEM-EUSO.

2 Neutrino nucleon interaction

High energy neutrinos that propagate in the Earth atmosphere can interact with protons and neutrons of the air molecules. There are two possible channels for this interaction, charged and neutral current, $\nu_l + N \to l + X$ and $\nu_l + N \to \nu_l + X$, respectively. Here N is a nucleon (proton or neutron), ν_l is a neutrino of family l, l is the corresponding lepton and X the hadronic part of the processes. At the level of the quark-parton model, the entire hadronic state of a deep inelastic scattering may be viewed as the fragmented product of a scattered quark and the proton remnant. The major uncertainty on the

differential cross section at the energies considered comes from the unknown behavior of the parton distribution functions (PDFs) at very small values of the parton momentum fraction x [13].

In this work, the simulation of the neutrino nucleon interaction is performed by using the PYTHIA code [14]. PYTHIA is an event generator, intended for high-energy processes with particular emphasis on the detailed simulation of quantum chromodynamics (QCD) parton showers and the fragmentation process.

The parton shower approach was developed to take into account higher than first order QCD effects. It has the advantage that arbitrarily high orders in the strong coupling constant can be simulated, but only in the leading order approximation, as opposed to the exact treatment in fixed order matrix element. Higher order effects are important at high energies where multiple parton emission can give rise to multijet events as well as affect the internal properties, such as hardness and width, of a jet (see Ref. [15]).

QCD perturbation theory, formulated in terms of quarks and gluons, is valid at short distances. At long distances, it becomes strongly interacting and perturbation theory breaks down. As mentioned before, in this confinement regime, the colored partons are transformed into colorless hadrons. The fragmentation process has yet to be understood from first principles, starting from the QCD Lagrangian. As a consequence, a number of different phenomenological models have been developed to describe this effect. In PYTHIA the fragmentation process is done by using the so-called Lund string model [16].

A typical high energy event has the following structure [14]:

(1) At the beginning of the simulation two incident beams are coming in towards each other. Each particle is characterized by a set of PDFs which determines the fraction of momentum taken by each parton.
(2) A collision between two partons, one from each beam, gives the hard process of interest. A collision implies accelerated color (and often electromagnetic charges), therefore, bremstrahlung can occur. The colliding partons start off a sequence of branchings (such $q \to qg$, $g \to gg$, $g \to q\bar{q}$, etcetera) which build up an initial-state shower.
(3) Also the outgoing partons may branch to build up a final-state shower.
(4) At this stage just one parton of each incident beam is taken out to undergo a hard collision. The beam particles are made up of a multitude of further partons, then, a beam remnant is left behind. This remnant may have an internal structure and a net color charge.
(5) The QCD confinement mechanism ensure that the outgoing quarks and gluons are not observable, but instead they fragment to color neutral hadrons.

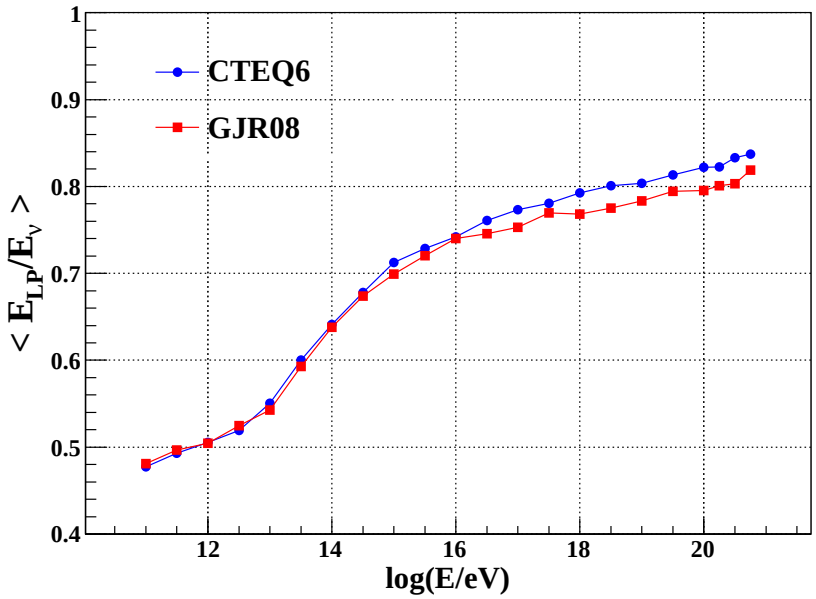

Fig. 1. Average energy fraction taken by the electron in a proton-electron neutrino charge current interaction obtained from PYTHIA with CTEQ6 (circles) and GJR08 (squares) sets of PDFs.

(6) Many of those primary hadrons are unstable and decay further at various time scales.

The default configuration of PYTHIA is used in the present simulations. Also, the parton distribution library LHAPDF [17] is linked with PYTHIA to use different extrapolations of the PDFs. In order to study the influence of the PDFs on the electron neutrino showers, two different sets are considered: CTEQ6 [18], the most commonly used in the literature (at the highest energies) and GJR08 [19]. Fig. 1 shows the energy fraction carried by the electron as a function of the incident neutrino energy for the charge current interaction of an electron neutrino with a proton for both sets of PDFs considered. In both cases the energy fraction increases steadily with the incoming neutrino energy. The difference between both PDFs increases up to a maximum of a few percent at the highest energies. Fig. 2 shows the distribution of the energy fraction taken by the electron for a neutrino of $E_\nu = 10^{20}$ eV interacting with a proton corresponding to CTEQ6. On average, approximately 82% of the neutrino energy is taken by the electron.

Besides the leading particle, different types of secondaries are generated as a result of the interaction. In particular, in this work we are interested in the ones recognized by CONEX [20] code which is used to simulate the neutrino showers (see section 3). The few final state particles that are not treated yet by CONEX are mapped into their decay products [21]. Fig. 3 shows the energy fraction taken by the most relevant particles recognized by CONEX for three

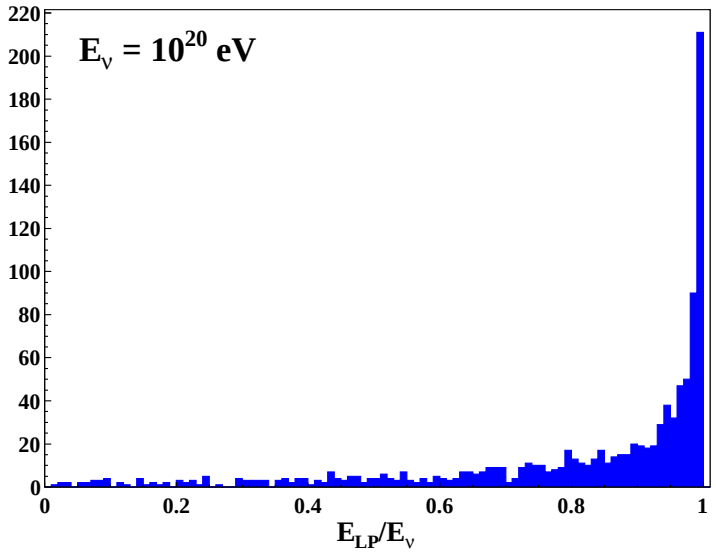

Fig. 2. Distribution of the energy fraction taken by the electron in a electron neutrino proton interaction. The neutrino energy is $E_\nu = 10^{20}$ eV and PYTHIA with CTEQ6 sets of PDFs are used for the simulations. The number of simulated events is 1000.

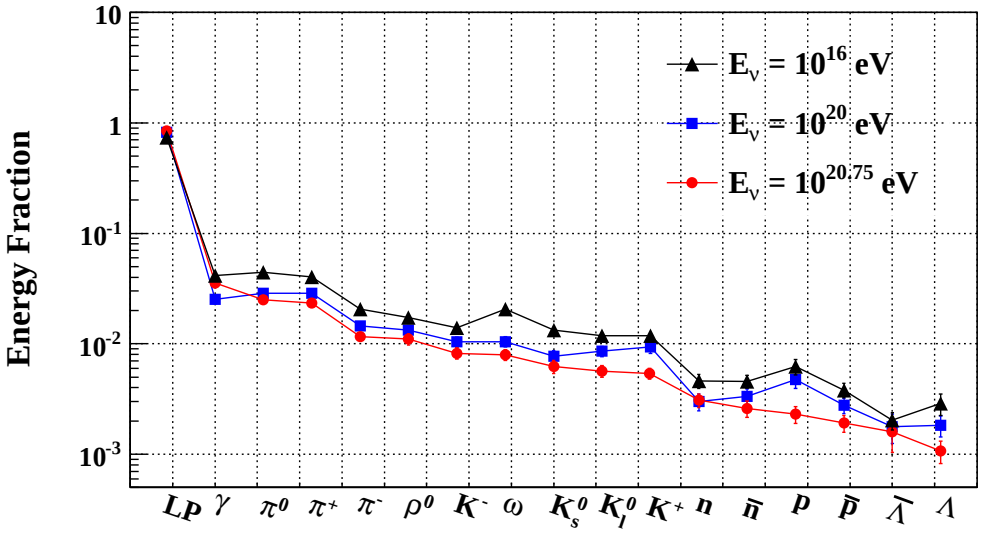

Fig. 3. Average energy fraction for the most important particles recognized by CONEX produced in a charge current interaction of an electron neutrino with a proton for three different neutrino energies.

different electron neutrino energies, obtained as a result of the charge current interaction with a proton. It can be seen that the smaller the neutrino energy the larger the energy fraction taken by the secondary particles.

Note that the results obtained for electron neutrinos are also valid for electron antineutrinos because at the energies considered in this work the cross-sections

are approximately the same (see for instance Ref. [22]).

3 Neutrino showers

There are several method to study the development of the extensive air showers. The most common one is the Monte Carlo (MC) simulation of the interactions suffered by the primary and the secondary particles of the showers with the air molecules. The MC programs most used in the literature are CORSIKA [23] and AIRES [24]. At the highest energies, the number of particles of the cascades is extremely large, e.g. $\sim 10^{11}$ particles at the maximum of a 10^{20} eV proton shower. The computing time required to simulate the interactions of all particles is so large that sampling algorithms, so-called "thinning", are used [25,26]. They are such that just a small fraction of the particles are propagated and a weight factor is associated to each of them. In these MC programs, both, the lateral and the longitudinal development of the showers are simulated.

The hybrid approach is a possible alternative to speed up the simulation of the showers without losing accuracy. It consists in the detailed MC simulation of the cascade for particles with energy above a given threshold and a description of the low energy sub-showers based on the numerical solution of the corresponding cascade equations.

As mentioned before the CONEX program is used to generate the electron neutrino showers. CONEX is a one-dimensional hybrid program which can be used to simulate the longitudinal profile of the showers very fast and very accurately. The accuracy of the calculation is supported by comparisons done between CONEX simulations and CORSIKA ones (see Ref. [20] for details). Note that the lateral development of the showers, not included in CONEX, is not important for the observation from the space, the showers are very well approximated by a point for the distances involved in this kind of techniques.

The major uncertainty for the shower simulations comes from the unknown of the hadronic interactions at the highest energies. There are several models that extrapolate the accelerator data to the energies of the cosmic rays, one of those is QGSJET-II [27] which is the one used in this work. The development of the shower strongly depends on the assumed hadronic interaction model. In particular, the most important observables of the showers, like the position of the maximum and the muon content, are quite sensitive to the hadronic interaction model considered (see Ref. [28,29] for details).

The particles produced in a neutrino-nucleon interaction are injected in CONEX with QGSJET-II producing extensive air showers. The energy thresholds used

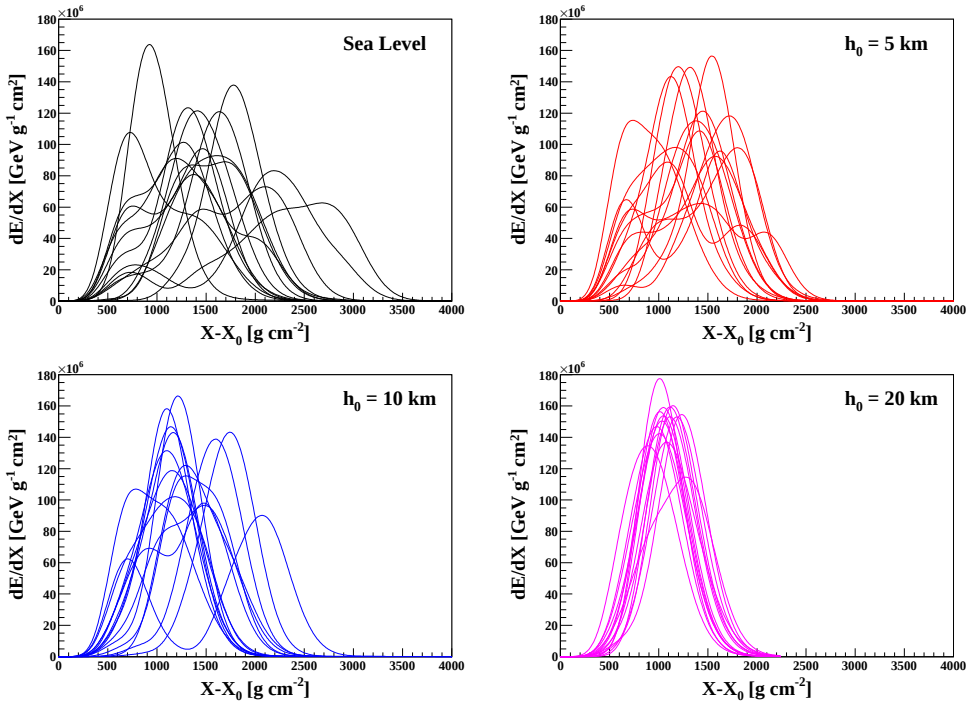

Fig. 4. Horizontal electron neutrino showers at four different altitudes of $E_\nu = 10^{20}$ eV, injected at a point contained on the vertical axis of a nadir-pointing orbital detector. $N = 15$ profiles are shown for every value of altitude considered.

in the present simulations are the ones suggested by the authors of the program, i.e. default configuration.

Because the mean free path of neutrinos propagating in the atmosphere is very large, they can interact very deeply, after traversing a large amount of matter. An orbital detector like JEM-EUSO can also detect horizontal showers that do not hit the ground. In particular, horizontal neutrinos can interact at higher altitudes producing a shower observable by the detector. Fig. 4 shows the energy deposit as a function of $X - X_0$, where X_0 corresponds to the atmospheric depth of the injection point, for horizontal electron neutrino showers of $E_\nu = 10^{20}$ eV. The injection points are such that the trajectory of the showers starts at the vertical axis of a nadir-pointing orbital telescope (like JEM-EUSO in nadir mode, see section 4) and at different altitudes. Note that, because of the very large mean free path of neutrinos in the atmosphere, a subset of all possible neutrino interactions inside the field of view (FOV) of the detector can be modeled by this kind of trajectories. Also note that for an horizontal proton shower of $E = 10^{20}$ eV the maximum is reached at $X \cong 890$ g cm^{-2}, with an energy deposit of $\sim 1.65 \times 10^8$ GeV g^{-1} cm^2.

As seen from fig. 4, the profiles corresponding to smaller altitudes are very broad profiles which may present several peaks and large fluctuations. This behavior is due to the Landau Pomeranchuk Migdal (LPM) effect, which is

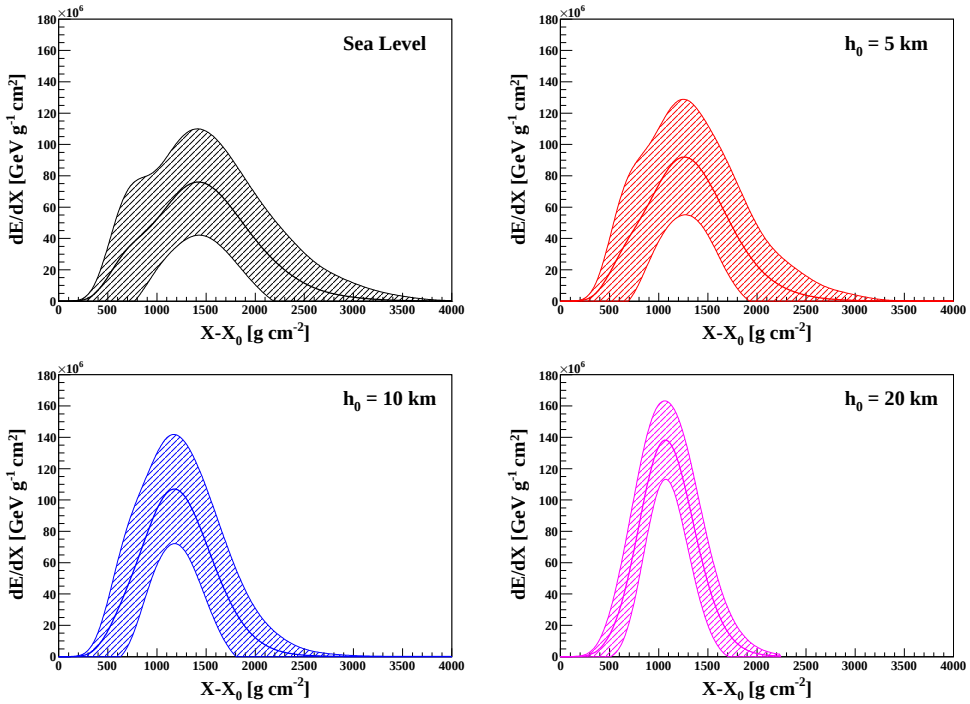

Fig. 5. Mean value and one sigma regions of the longitudinal profile corresponding to horizontal electron neutrino showers of $E_\nu = 10^{20}$ eV for different altitudes. The interaction point is contained on the vertical axis of the JEM-EUSO telescope.

very important inside dense regions of the atmosphere and for electromagnetic particles, electrons in this case, which take about 80% of the parent neutrino energy. Fig. 5 shows the mean value and one sigma regions of the longitudinal profiles for the same geometry and injection point considered before. It can be seen that as the altitude increases the fluctuations are reduced and, on average, the profiles become thinner. This is due to the fact that the LPM effect become progressively less important with increasing altitude because of the decrease in atmospheric density. Note that just showers up to 20 km of altitude are considered because, at higher altitudes, the grammage of the FOV like the one of JEM-EUSO, 60°, is not enough to contain the whole profiles.

As already mentioned, at smaller altitude the longitudinal profiles present a complicated structure (see Fig. 4). In particular, the showers present multiple peaks. Fig. 6 shows the distributions functions of the position of each maximum. X^1_{max} corresponds to the position of the first maximum counted from the start of the shower, X^2_{max} is the second one and so on. The maxima are obtained by searching for the points of the longitudinal profile which have six consecutive neighbors, three with atmospheric depth smaller and three with atmospheric depth larger. These six points are such that the deposited energy is smaller than the one of the candidate. When a candidate is found, the coordinates of the maximum are obtained by using a parabola that fit the central point and the two nearest neighbors, one at the right and the other at the left.

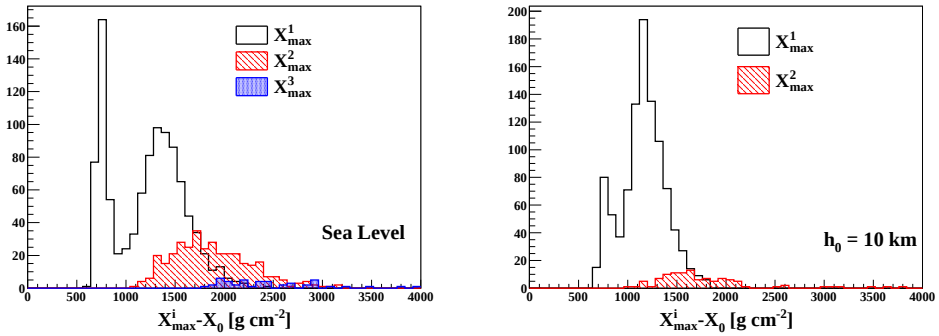

Fig. 6. Distribution of the position of the maxima for electron neutrino showers of $E_\nu = 10^{20}$ eV at sea level.

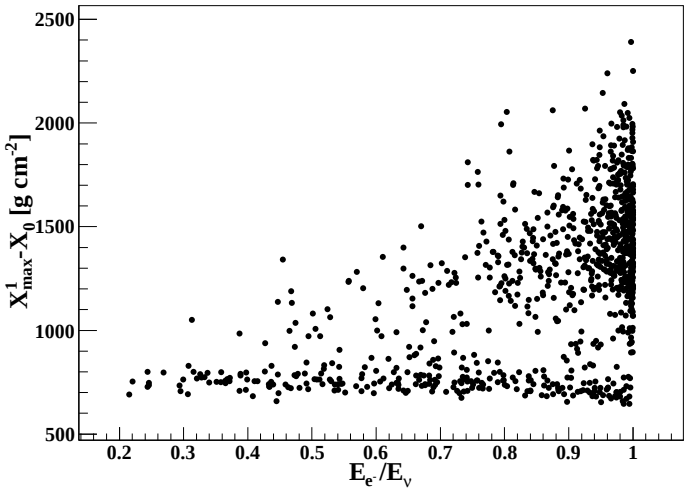

Fig. 7. $X^1_{max} - X_0$ as a function of the fractional energy taken by the electron, for neutrino showers of $E_\nu = 10^{20}$ eV at sea level.

Note that the distribution function of $X^1_{max} - X_0$ is bi-valued and its first peak is located at ~ 800 g cm^{-2}, while the second one is centered at ~ 1500 g cm^{-2}. The first peak corresponds to the development of the hadronic component of the electron neutrino cascade, whereas the second one mainly reflects the electromagnetic portion of the shower. Fig. 7 shows $X^1_{max} - X_0$ as a function of the energy fraction taken by the electron, it can be seen that, as the fractional energy of the electron decreases $X^1_{max} - X_0$ of the events approaches to the values corresponding to the first peak.

The interpretation of the $X^1_{max} - X_0$ distribution can be confirmed by simulating the shower development removing the hadronic component produced in the neutrino nucleon interaction, i.e. considering just the generated electron. The distribution of $X^1_{max} - X_0$ for the electron showers obtained applying the

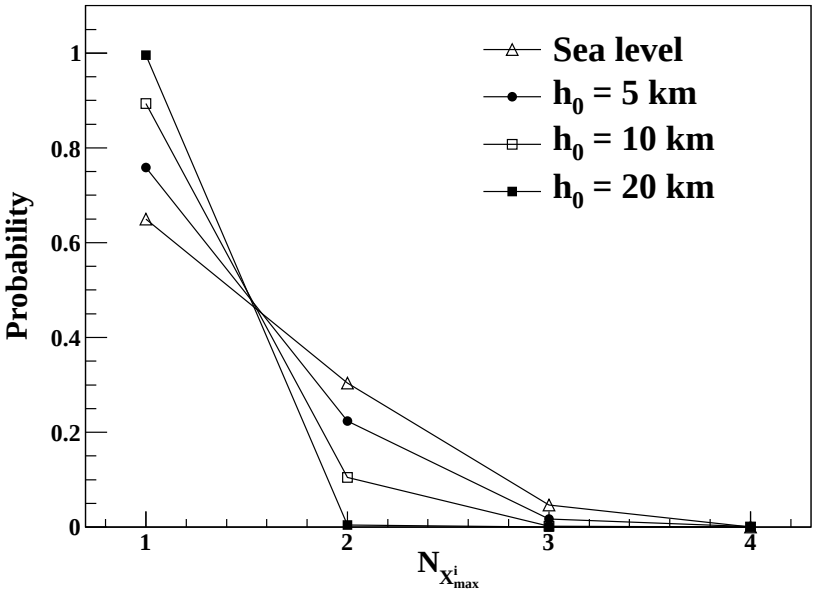

Fig. 8. Probability of an electron neutrino shower to have $N_{X^i_{max}}$ maxima for $E_\nu = 10^{20}$ eV for horizontal showers at different altitudes.

same analysis as before do not present the first peak, as expected it just have one peak at ~ 1500 g cm^{-2} (see Fig. A.1 of appendix A).

The simulations show that $\sim 65\%$ of the showers that have a second maximum have $X^1_{max} - X_0 \leq 1000$ g cm^{-2}. Therefore, as mentioned before, the distribution of $X^2_{max} - X_0$ has to do with the electromagnetic part of the showers. When the first maximum is in the electromagnetic region of the distribution, the second one is originated by the fluctuations due to the LPM effect. This is supported by the $X^2_{max} - X_0$ distribution of the electron showers discussed in the appendix A, it is originated by the LPM fluctuations and, as expected, corresponds to larger values of $X^2_{max} - X_0$ (see Fig. A.1). The third maximum (X^3_{max}) is always originated by the fluctuations caused by the LPM effect.

This complicated structure simplifies as the altitude increases. Fig. 8 shows the probability of finding a profile with a given number of peaks, $N_{X^i_{max}}$. As the altitude increases the probability of finding a shower with more than one peak goes to zero.

The first portion of the cascades is, in general, dominated by the hadronic component. Therefore, the way in which the primary neutrino energy is distributed can be assessed by,

$$F_{en} = \frac{\int_0^{X_c} dX \, \frac{dE}{dX}}{\int_{X_c}^{X_{lim}} dX \, \frac{dE}{dX}}, \tag{1}$$

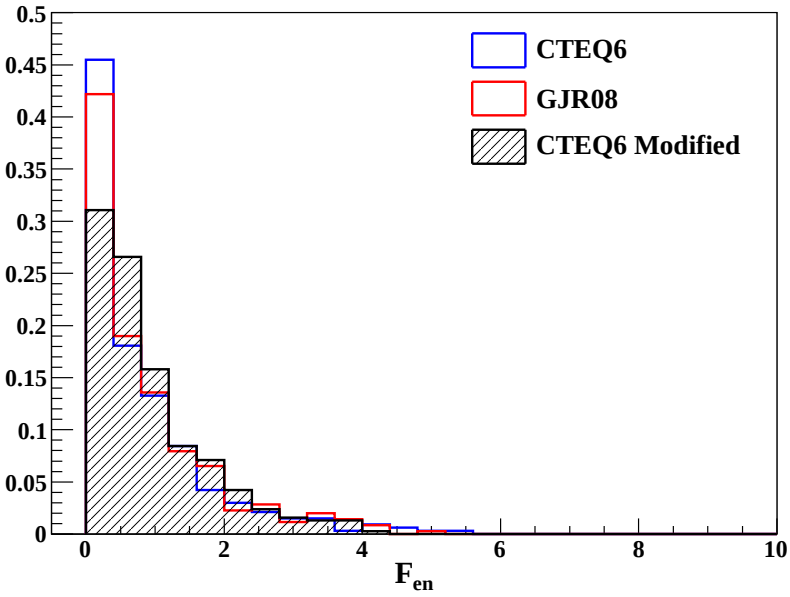

Fig. 9. Distribution function of parameter F_{en} (see Eq. (1)) for CTEQ6, GJR08 models and also for an artificial modification of the CTEQ6 prediction such that the leading particle takes 70% of the neutrino energy. Horizontal showers of 10^{20} eV injected at sea level at the axis of the FOV are considered.

where dE/dX is the energy deposition, $X_c = 1000$ g cm^{-2} is a characteristic depth that roughly separates the hadronic-dominated from the electromagnetic-dominated portions of the shower (see Fig. 6), and X_{lim} is the maximum atmospheric depth visible by a given orbital detector. F_{en} is calculated only for those showers that present a first maximum at a depth smaller than X_c. Fig. 9 shows the F_{en} distributions obtained for CTEQ6, GJR08 and for a modification of the CTEQ6 results in which the leading particle takes 70% of the neutrino energy, corresponding to horizontal 10^{20} eV electron neutrinos injected at sea level at the axis of the FOV. It can be seen that F_{en} is correlated with the energy taken by the leading particle. The smallest value of the average of F_{en} corresponds to CTEQ6 because the leading particle takes about 82% of the neutrino energy while, in the case of GJR08, it takes $\sim 79\%$. The differences between the results obtained for these models are very small. In the case in which the energy taken by the leading particle is artificially reduced to 70% (hashed histogram), the mean value of F_{en} increases. Note that, in the latter case, the energy extracted from the leading particle in order to reduce its average energy, is redistributed among the other daughter particles in such a way that the ratio between the energy taken by a given particle and the total energy taken by all secondaries, excluding the leading particle, is constant.

Figures 7 and 9 show the influence of the energy taken by the hadronic component of the neutrino interaction on the hadronic character of the beginning of electron neutrino showers. In fact, the position of $X^1_{max} - X_0$ as well as the

energy deposition at the beginning part of the showers are correlated with the amount of energy that goes to this component.

The sensitivity of F_{en} to the hadron component of the showers depends on the altitude. Showers injected at sea level in regions of high density are dominated by the LPM effect allowing a clearer separation between the hadronic and electromagnetic portions of the cascades.

The parameter F_{en} can be very useful to understand neutrino interactions with atmospheric nuclei and, in particular, to estimate the energy fraction taken by the leading particle. Any practical application, however, will depend on the actual event rate.

4 Detectability for an ideal orbital detector

As mentioned before, a new generation of orbital detectors are planned. Such instruments are designed to detect the fluorescence light emitted by the interaction of the charge particles of the air showers initiated by the primary cosmic rays. These new instruments, of which JEM-EUSO is the pioneer, watch the atmosphere from the space, having a huge effective area. In particular, JEM-EUSO will watch the atmosphere in two different ways, nadir and tilted modes. The telescope is formed by three double-sided Fresnel lenses made of plastic material and an aspherically curved focal surface composed by multi-anode photomultipliers to detect the incident photons [30].

A simplified simulation of an orbital detector with characteristics similar to JEM-EUSO is developed, in order to study the detectability of the electron neutrino showers. The simulation of the fluorescence light emitted by the charged particles of the cascades is done by using the photon yield of Ref. [31]. The fluorescence light is propagated from the shower axis to the telescope considering the Rayleigh and Mie attenuation [32]. An ideal optical system is considered, an optical transmission of 100% is assumed independent of the angle and wavelength of the incident light. Regarding the PMTs a combined collection efficiency and quantum efficiency of $\epsilon_{pmt} = 0.27$ is considered [33]. The Cherenkov photons are not included in the present simulations, for the case of horizontal showers this component is less important because such photons are very collimated with the shower axis and just the scattered ones can contribute to the light collected by the telescope. Also the attenuation of the fluorescence light due to the ozone absorption is not included in the simulation.

Table 4 shows the parameters used in the simulation of the ideal orbital detector (see Ref. [34]).

Parameter	Value
Height of the orbit	400 km
Aperture diameter (D_A)	2.5 m
Field of View	$\pm 30^\circ$
Wavelength range	$330 - 400$ μm
Gate Time Unit (GTU)	2500 ns
Number of pixels (N_{pix})	2×10^5
Pixel size	0.1°

Table 1
Parameters used in the simulation of an ideal orbital detector similar to JEM-EUSO.

The main source of background light is the atmospheric nightglow, the mean value assumed in this work is $B_0 = 500$ photons m^{-2} ns^{-1} sr^{-1} [30]. The rate of background photons per pixel is given by,

$$R_b = \frac{\pi\ \epsilon_{pmt}\ A\ B_0\ \sin^2\gamma_{fov}}{N_{pix}}, \tag{2}$$

where $A = \pi D_A^2/4$ and $\gamma_{fov} = 30^\circ$ (γ is used to note the angle between the incident light and the axis of the telescope).

Figure 10 shows the number of photons that produce signal in the PMTs as a function of the arrival time, for two different events corresponding to horizontal electron neutrino showers injected at sea level in the center of the FOV of the telescope. The temporal width of each bin is equal to a GTU. The black lines, $N(k)$, correspond to 3 (solid line) and 5 (dashed line) sigmas above the background in the corresponding time bins. Assuming Poissonian statistics and for k sigmas above the mean in the ith bin, $N_i(k) = k\ \sqrt{N_i^b}$, with $N_i^b = R_b \times \mathrm{GTU} \times \Delta\gamma_i/0.1^\circ$, where $\Delta\gamma_i/0.1^\circ = (\gamma(t_i + \Delta t_i) - \gamma(t_i))/0.1^\circ$ is the fraction of the pixel corresponding to the ith time bin. The separation between two consecutive dotted vertical lines indicates the time interval corresponding to an angular separation of 0.5°, i.e. five pixels.

The event on the left panel of Fig. 10 presents just one peak, it has several pixels with the number of photons well above the background, 12 above $3\,\sigma$ and $5\,\sigma$. The event on the right panel of the same figure has two peaks, in this case the photons are distributed in a wider interval of time due to the shape of the longitudinal profile. Also in this case there are several pixels with the number of photons above the background, 23 above $3\,\sigma$ and 18 above $5\,\sigma$.

As the altitude increases the distribution of photons changes. Fig. 11 shows two events corresponding to $h_0 = 5$ km, it can be seen that the number of photons that produce signal in the PMTs increases because the distance of the

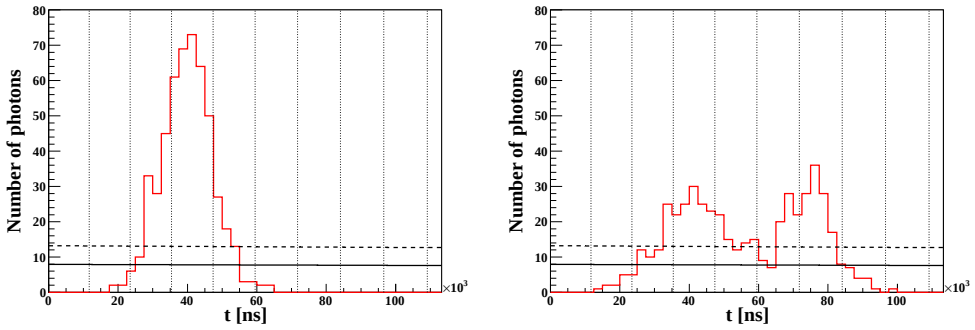

Fig. 10. Time distribution of photons that produce signal in the PMTs for two electron neutrino horizontal showers of $E_\nu = 10^{20}$ eV, injected at sea level in the center of the FOV of an orbital telescope. The set of PDF used is CTEQ6.

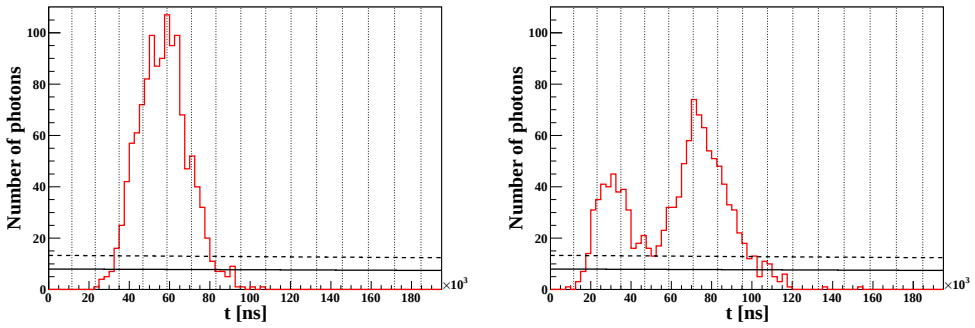

Fig. 11. Time distribution of photons that produce signal in the PMTs for two electron neutrino horizontal showers of $E_\nu = 10^{20}$ eV, injected at an altitude of $h_0 = 5$ km in the center of the FOV of an orbital telescope. The set of PDF used is CTEQ6.

shower to the telescope is smaller, increasing the solid angle of the photons that reach the telescope and decreasing the attenuation in the atmosphere. Also the angular width of the distribution increases due to geometrical effects. As a result, the number of pixels with the number of photons larger than a given level of background increases. As expected, the detectability of the horizontal showers improves for larger altitudes. For the event on the left panel of the figure there are 22 pixels above $3\,\sigma$ and 20 pixels above $5\,\sigma$ and for the event on the right panel there are 38 pixels above $3\,\sigma$ and 33 pixels above $5\,\sigma$.

Figure 12 shows the distribution of photons for showers injected at $h_0 = 10$ km and $h_0 = 20$ km. Again, the number of pixels with signal well above a given background level increases with altitude in such a way that, for $h_0 = 10$ km (left panel) there are 44 pixels above $3\,\sigma$ and 39 pixels above $5\,\sigma$. For the event corresponding to $h_0 = 20$ km (right panel) there are 187 pixels above $3\,\sigma$ and 171 pixels above $5\,\sigma$.

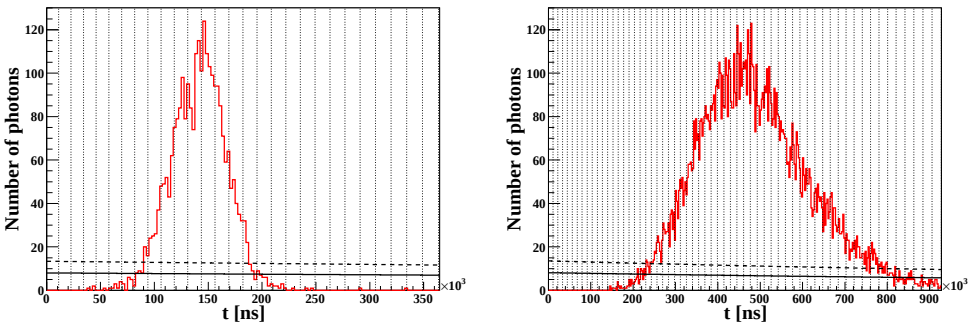

Fig. 12. Time distribution of photons that produce signal in the PMTs for two electron neutrino horizontal showers of $E_\nu = 10^{20}$ eV, injected at $h_0 = 10$ km (left panel) and $h_0 = 20$ km (right panel) in the center of the FOV of an orbital telescope. The set of PDF used is CTEQ6.

5 Proton and neutrino showers

The interaction length for protons is $\lambda_{pr}(10^{20}\text{eV}) \sim 36$ g cm^{-2} (for Sibyll 2.1 [36]) and for neutrinos is $\lambda_\nu(10^{20}\text{eV}) \sim 3.2 \times 10^7$ g cm^{-2}. The survival probability of an horizontal proton that reaches the Earth surface at the vertical axis of the FOV is $\sim \exp(-1000)$, whereas the corresponding probability for a neutrino is $\sim \exp(-0.001)$. Therefore, despite the fact that horizontal neutrino and proton showers have very different observational characteristics, it is very unlikely to observe a proton interacting so deep in the atmosphere.

Nevertheless, for a given proton and a neutrino fluxes, there exists a particular slant depth for which the proton and neutrino events have the same rate. For any particle type, the probability of interacting in the interval $[X, X + \Delta X]$ is given by,

$$P_{int}(E; X, \Delta X) = \exp(-X/\lambda(E)) \ \left[1 - \exp(-\Delta X/\lambda(E))\right], \tag{3}$$

where $\lambda(E)$ is the interaction length at a given energy. Therefore, solving the equation $\phi_{pr}(E)\ P^{pr}_{int}(E; X_0, \Delta X) = \phi_\nu(E)\ P^{\nu}_{int}(E; X_0, \Delta X)$, where $\phi_{pr}(E)$ and $\phi_\nu(E)$ are the proton and neutrino fluxes, the slant depth at which protons and neutrinos can be detected with the same rate is,

$$X(E) = \frac{\lambda_{pr}(E)\lambda_\nu(E)}{\lambda_{pr}(E) - \lambda_\nu(E)} \left[\ln\left(\frac{\phi_\nu(E)}{\phi_{pr}(E)}\right) + \ln\left(\frac{1 - \exp(-\Delta X/\lambda_\nu(E))}{1 - \exp(-\Delta X/\lambda_{pr}(E))}\right)\right] \tag{4}$$

The function $X(E)$ is obtained by using: $\Delta X = \lambda_{pr}(E)$, the proton-air cross section of Sibyll 2.1, the charged current neutrino cross section $\sigma^{CC}_{N\nu}(E) = 6.04 \times 10^{-36}\ (E/\text{GeV})^{0.358}$ cm^2 [37], the Waxman-Bachall upper limit for the neutrino flux [38] and a power law fit of the Auger spectrum [39]: $\phi_{pr}(E) \cong 3.64 \times 10^{38}\ (E/\text{eV})^{-3.733}$ m^{-2} s^{-1} sr^{-1} eV^{-1}. Therefore, for $E = 10^{20}$ eV the

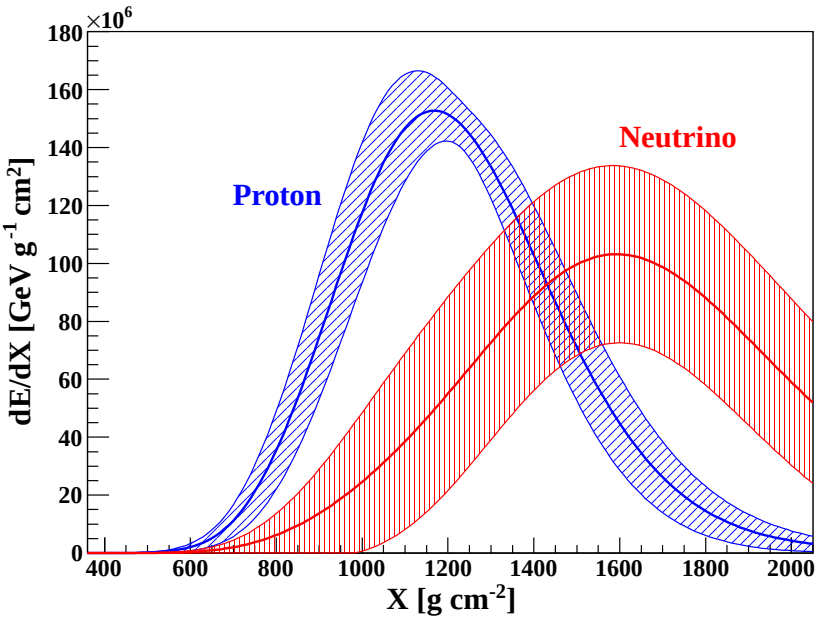

Fig. 13. Proton and electron neutrino air showers of 10^{20} eV, $\theta = 60°$ injected at 360 g cm^{-2}.

event rate for protons and neutrinos are of the same order of magnitude for $X \cong 360$ g cm^{-2} (where $\phi_\nu(10^{20}\text{eV}) \cong 2 \times 10^{-35}$ m^{-2} s^{-1} sr^{-1} eV^{-1} and $\phi_{pr}(10^{20}\text{eV}) \cong 8 \times 10^{-37}$ m^{-2} s^{-1} sr^{-1} eV^{-1}). The latter means that, under the assumptions of the present calculation, protons can act as a background for neutrino identification in inclined events. Note that for values low enough of the neutrino flux, which could be the case, there is no atmospheric depth for which both rates are the same.

Fig. 13 shows the average profile and the one sigma region for proton and electron neutrino induced air showers of zenith angle $\theta = 60°$ and primary energy 10^{20} eV injected at 360 g cm^{-2}. Although, the event rates of this kind of showers are similar by assumption, for both protons and neutrinos, the profiles, however, are quite different making possible a good discrimination. More specifically, it can be seen that the neutrino showers develop deeper in the atmosphere and present larger fluctuations, due to the LPM effect.

6 Conclusions

Neutrino detection is of great importance for the understanding of several astrophysical process and, in particular, the origin and propagation of the highest energy cosmic rays. Orbital detectors like JEM-EUSO are technically capable of observing neutrino initiated cascades and to discriminate these cascades from hadronic ones.

Horizontal electron neutrino showers interacting very deep in the atmosphere are dominated by the LPM effect. The characteristics of such showers depend strongly on the density of the atmosphere and consequently on the altitude at which they develop. We show that horizontal electron neutrino showers interacting at sea level can present several peaks and large fluctuations. As the altitude increases the probability of finding a profile with more than one peak decreases. Also the fluctuations decrease with altitude. We find that the detectability of this kind of showers, in the context of an orbital telescope, improves with altitude and the multiple peak structure can be observed by this type of detectors. We also show that protons are a possible background for the neutrino identification depending on the unknown neutrino flux. However, even for optimistic values of such flux the longitudinal profiles are different enough to allow a good discrimination.

7 Acknowledgments

This work is part of the ongoing effort for the design and development of the JEM-EUSO mission and the definition of its scientific objectives. The authors acknowledge the support of UNAM through PAPIIT grant IN115707 and CONACyT through its research grants and SNI programs. ADS is supported by a postdoctoral grant from the UNAM.

A Electron showers

Electron showers are generated injecting in CONEX just the electron generated in the electron neutrino nucleon interaction simulated with PYTHIA. The distributions of $X^i_{max} - X_0$ are obtained by using the same method described in section 3. Figure A.1 shows that, in this case, the distribution of the first maximum just has one peak at ~ 1500 g cm^{-2}.

References

[1] M. Kachelriess, S. Ostapchenko, and R. Tomas, arXiv:0805.2608.

[2] V. Berezinsky and G. Zatsepin, Phys. Lett. **28B**, 423 (1969).

[3] Allard et al., JCAP **0609**, 5 (2006).

[4] D. Fargion, A. Aiello, and R. Conversano, Proceedings of 26th ICRC 1999, 396-398 (1999).

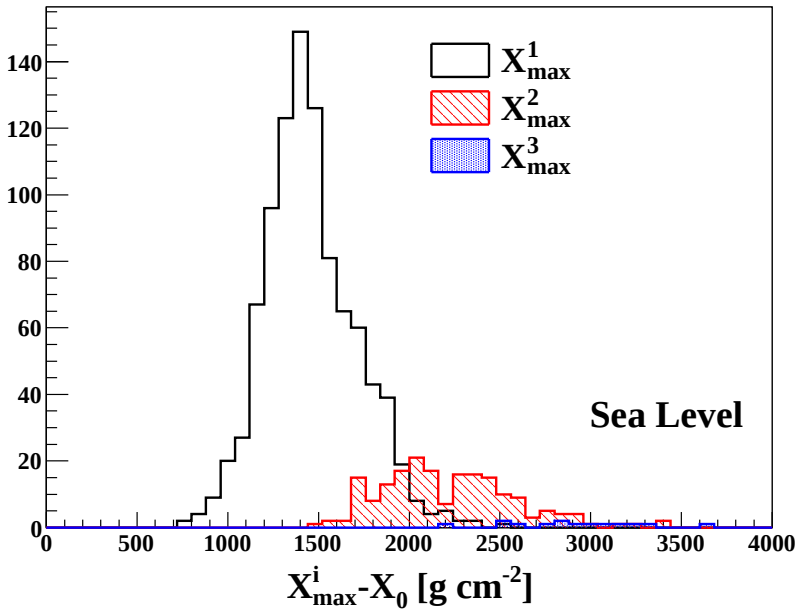

Fig. A.1. Distribution of the position of the maxima for horizontal electron showers at sea level. The electrons are generated in the neutrino nucleon interactions corresponding to $E_\nu = 10^{20}$ eV with CTEQ6 as PDF.

[5] D. Fargion, Astrophys. J. **570**, 909 (2002).

[6] D. Fargion, P.G. De Sanctis Lucentini, M. De Santis, and M.Grossi, Astrophys. J. **613**, 1285 (2004).

[7] V. Berezinsky and A. Smirnov, Ap. Sp. Sci. **32**, 461 (1975).

[8] R. Aloisio, V. Berezinsky, and M. Kachelriess, Phys. Rev. **D69**, 094023 (2004).

[9] P. Battacharjee and G. Sigl, Phys. Rept. **327**, 109 (2000).

[10] T. Ebisuzaki, Nucl. Phys. **B** 175-176, 237-240 (2008). T. Ebisuzaki, Proceedings of 31st ICRC 2009, #1035.

[11] G. Medina-Tanco et al., Proceedings of 31st ICRC 2009, #529.

[12] S. Palomares-Ruiz, A. Irimia, and T. Weiler, Phys. Rev. **D73**, 083003 (2006).

[13] M. M. Block, P. Ha and D. W. McKay, Phys. Rev. **D82** 077302 (2010).

[14] T. Sjostrand, S. Mrenna, and P. Skands, JHEP **0605**, 026 (2006).

[15] T. Sjostrand, arXiv:0911.5286.

[16] B. Andersson, G. Gustafson, G. Ingelman and T. Sjostrand, Phys. Rep. **97**, 31 (1983).

[17] M. Whalley, D. Bourilkov, and R. Group, http://hepforge.cedar.ac.uk/lhapdf/.

[18] P. Nadolsky et al., Phys. Rev. **D78**, 013004 (2008).

[19] M. Gück, P. Jimenez-Delgado, and E. Reya, Eur. Phys. J. **C53**, 355 (2008).

[20] T. Bergmann et al., Astropart. Phys. **26**, 420 (2007).

[21] M. Ambrosio et al., Proceedings of 28th ICRC 2003. M. Ambrosio et al., arXiv:astro-ph/0302602.

[22] R. Gandhi, C. Quigg, M. Reno, and I. Sercevic, Astropart. Phys. **5**, 81 (1996).

[23] D. Heck *et al.*, Report **FZKA 6097**, Forschungszentrum Karlsrue, 1998; http://www-ik3.fzk.de/∼/heck/corsika.

[24] S. Sciutto, AIRES user's Manual and Reference Guide (2002), http://www.fisica.unlp.edu.ar/auger/aires.

[25] A. Hillas, Proc. 19th ICRC **1**, 155 (1985).

[26] A. Hillas, Nucl. Phys. (Proc. Suppl.) **B52**, 29 (1997).

[27] S. Ostapchenko, Nucl. Phys. Proc. Suppl. **B151**, 143 (2006).

[28] R. Ulrich et al., Proceedings of 31st ICRC 2009, #734.

[29] R. Ulrich, R. Engel, and M. Unger, arXiv:1010.4310.

[30] Y. Takahashi and the JEM-EUSO Collaboration, New J. Phys. **11**, 065009 (2009).

[31] M. Nagano et al., Astropart. Phys. **22**, 235 (2004).

[32] P. Sokolsky, Introduction to Ultrahigh Energy Cosmic Ray Physics, Addison-Wesley, Reading, MA, 1989.

[33] F. Fenu et al., Proceedings of 31st ICRC 2009, #1357.

[34] K. Shinozaki et al., Proceedings of 31st ICRC 2009, #389.

[35] F. Kajino for the JEM-EUSO Collaboration, Proc. 30st ICRC **5**, 1077 (2007).

[36] R. Engel, T. Gaiser, P. Lipari, and T. Stanev, Proc. 26th ICRC **1**, 415 (2000).

[37] L. Anchordoqui, A. Cooper-Sarkar, D. Hooper, and S. Sarkar, Phys. Rev. **D74**, 043008 (2006).

[38] E. Waxman and J. Bahcall, Phys. Rev. **D59**, 023002 (1999).

[39] J. Abraham et al., Phys. Rev. Lett. **101**, 061101 (2008).